Available online at www.sciencedirect.com
ScienceDirect
Journal of Solid State Chemistry 180 (2007) 3341–3350
JOURNAL OF SOLID STATE CHEMISTRY
www.elsevier.com/locate/jssc

Cobalt–silicon mixed oxide nanocomposites by modified sol–gel method

Serena Esposito[a], Maria Turco[b], Gianguido Ramis[c], Giovanni Bagnasco[b], Pasquale Pernice[d], Concetta Pagliuca[a], Maria Bevilacqua[c], Antonio Aronne[d,*]

[a]*Laboratorio Materiali del Dipartimento di Meccanica, Strutture, Ambiente e Territorio, Facoltà di Ingegneria dell'Università di Cassino, Via G. di Biasio 43, I-03043 Cassino (Fr), Italy*
[b]*Dipartimento di Ingegneria Chimica, Università di Napoli Federico II, P.le Tecchio, I-80125 Napoli, Italy*
[c]*Dipartimento di Ingegneria Chimica e di Processo "G.B. Bonino", Università di Genova, P.le J.F. Kennedy, I-16129 Genova, Italy*
[d]*Dipartimento di Ingegneria dei Materiali e Produzione, Università di Napoli Federico II P.le Tecchio, I-80125 Napoli, Italy*

Received 4 July 2007; received in revised form 11 September 2007; accepted 29 September 2007
Available online 4 October 2007

Abstract

Cobalt–silicon mixed oxide materials (Co/Si = 0.111, 0.250 and 0.428) were synthesised starting from $Co(NO_3)_2 \cdot 6H_2O$ and $Si(OC_2H_5)_4$ using a modified sol–gel method. Structural, textural and surface chemical properties were investigated by thermogravimetric/differential thermal analyses (TG/DTA), XRD, UV–vis, FT-IR spectroscopy and N_2 adsorption at −196 °C. The nature of cobalt species and their interactions with the siloxane matrix were strongly depending on both the cobalt loading and the heat treatment. All dried gels were amorphous and contained Co^{2+} ions forming both tetrahedral and octahedral complexes with the siloxane matrix. After treatment at 400 °C, the sample with lowest Co content appeared amorphous and contained only Co^{2+} tetrahedral complexes, while at higher cobalt loading Co_3O_4 was present as the only crystalline phase, besides Co^{2+} ions strongly interacting with siloxane matrix. At 850 °C, in all samples crystalline Co_2SiO_4 was formed and was the only crystallising phase for the nanocomposite with the lowest cobalt content. All materials retained high surface areas also after treatments at 600 °C and exhibited surface Lewis acidity, due to cationic sites. The presence of cobalt affected the textural properties of the siloxane matrix decreasing microporosity and increasing mesoporosity.

Keywords: Microporous materials; Sol–gel; Surface properties

1. Introduction

Systems based on cobalt oxide nanoparticles dispersed in amorphous high surface area silica matrix are receiving growing interest as gas sensors [1,2] or catalysts for hydrogenation–dehydrogenation reactions such as reforming of methane [3], ethene hydroformylation [4], hydrogenation of aromatics [5] and aldehydes [6], Fischer–Tropsch synthesis (FTS) [7–16]. FTS reaction appears of particular interest since it is the key step of biomass-to-liquid (BTL) process for the production of biofuels that are forecasted to replace a significant share of fossil fuels in the near future [17,18]. Several recent studies on cobalt–silica systems have shown that the preparation method and the structure of the silica matrix has a marked influence on the type and dispersion of cobalt oxide species, and thus on the properties of the derived catalysts [19–23]. Therefore, there is great interest for the study of new synthesis procedures of these materials as well as for the study of the interactions between the active phase and the silica matrix.

Many methods have been explored to disperse the cobalt oxide in the silica matrix that can be grouped in two categories: methods based on post-synthesis treatments of the silica matrix, such as ion-exchange [24,25], impregnation [26], grafting techniques [27] and methods involving simultaneous synthesis of cobalt and silicon oxides from suitable precursors, such as sol–gel with or without template molecules [9,16]. The sol–gel method appears preferable since it allows a better control of the textural properties of the silica matrix and a more effective

*Corresponding author. Fax: +39 081 76 82595.
E-mail address: anaronne@unina.it (A. Aronne).

0022-4596/$ - see front matter © 2007 Elsevier Inc. All rights reserved.
doi:10.1016/j.jssc.2007.09.032

dispersion of cobalt oxide in the matrix on a nanometric scale.

In this work, a modified sol–gel method [28] involving the hydrolysis of the Si and Co precursors in an almost solely aqueous environment was used to synthesise cobalt–silicon mixed oxide nanocomposites with different Co/Si ratios. Structural and textural properties of the materials are studied by different and complementary characterization techniques with the aim of obtaining information on the nature of cobalt oxide species and their interaction with the siloxane matrix.

2. Experimental

Cobalt–silicon mixed oxide nanocomposites with Co/Si = 0.111, 0.250 and 0.428 were prepared by a sol–gel method. The molar compositions of the gel-derived samples can be expressed also as $10Co \cdot 90SiO_2$ (10Co), $20Co \cdot 80SiO_2$ (20Co) and $30Co \cdot 70SiO_2$ (30Co). Cobalt nitrate hexahydrate, $Co(NO_3)_2 \cdot 6H_2O$ (Acros Organics), and tetraethoxysilane, $Si(OC_2H_5)_4$ (99%, ABCR) (TEOS) were used as starting materials.

TEOS (76 cm^3) was hydrolysed for 1 h at 50 °C without any alcoholic solvent using nitric acid (65%, 3 mmol) (Carlo Erba) as catalyst. The molar ratio employed was $TEOS:H_2O:HNO_3 = 1:4:0.01$. This solution was cooled to room temperature and $Co(NO_3)_2 \cdot 6H_2O$ (38, 85 and 145 mmol for 10Co, 20Co and 30Co, respectively) was slowly added under stirring. After 24 h transparent and pinkish coloured gels were obtained for each composition. The gelled systems were kept 3 days at room temperature before drying. The gels were fully dried in air at 110 °C in an electric oven for 12 h.

Pure silica (SiO_2) gel-derived glass was also synthesised by hydrolysing TEOS in the conditions described above.

The dried samples were annealed at different temperature ranging from 400 to 850 °C. Each sample was prepared by slow heating at 2 °C min^{-1} to the required temperature and then held at this temperature for 1 h followed by quenching. The heat-treated samples hereafter will be denoted with the labels indicating their nominal composition followed by the temperature of the heat treatment stage (10Co—400, 20Co—600, SiO_2—400, etc.).

Thermogravimetric/differential thermal analyses (TG/DTA) were carried out by using a Netzsch simultaneous thermoanalyser STA 409C with Al_2O_3 as reference material. The STA curves, recorded in air from room temperature up to 1000 °C at a heating rate of 10 °C min^{-1}, were carried out on 50 mg of the dried gels.

The amorphous nature of the dried gels as well as the nature of the crystallising phases was ascertained by X-ray diffraction with a Philips X'PERT diffractometer by using monochromatised Cu$K\alpha$ radiation (40 mA, 40 kV) with a step width of 0.02° 2θ, and 1 s data collection per step. The mean Co_3O_4 particle sizes were determined from the line broadening of the diffraction line at 36.8°, using the Scherrer equation.

The different configuration of the cobalt ions in the structure of the dried gels as well as of the gel-derived samples were evaluated by diffuse reflectance (DR) UV–vis spectroscopy using a Jasco spectrophotometer and $BaSO_4$ as a reference in the 200–800 cm^{-1} wavenumbers range. The measured intensity was expressed as the value of the Kubelka-Munk function $F(R)$.

Fourier transform (FT)-IR spectra of dried and heat-treated gel samples were carried out at room temperature by a Nicolet system, Nexus model, equipped with a DTGS KBr (deuterated triglycine sulphate with potassium bromide windows) detector. The absorption spectra were recorded in the 4000–400 cm^{-1} range with a spectral resolution of 2 cm^{-1}. Each test sample (2.0 mg) was mixed with 200 mg of KBr in an agate mortar, and then pressed into pellets of 13 mm diameter. The spectrum of each sample represents an average of 64 scans, which were corrected for the spectrum of the blank KBr. To allow the comparison of the absorbance values, all FT-IR spectra were normalised with respect to the maximum absorbance value recorded for each spectrum.

FT-IR spectra of NO adsorption were performed with a Nicolet Protegè 460 Fourier Transform spectrometer (4 cm^{-1} resolution) using self-supporting pressed disks of the pure powders, previously pre-treated by calcination in the IR cell at 400 °C for 2 h and outgassing at 400 °C for 30 min. The adsorption procedure involves contact of the activated samples disk with vapours (15 Torr) at r.t., heating at 100, 200 and 300 °C and outgassing in steps at r.t. and increasing temperatures up to 300 °C. The IR cell is connected to a conventional gas-handling system. The spectrum of the activated materials has been subtracted. NO was taken from commercial cylinder from SIAD (Milano, Italy) at 5×10^6 Pa, after careful purification by freezing and vacuum distillation. Its purity was checked by FT-IR and only few amounts of N_2O and NO_2 were detected.

N_2 adsorption–desorption isotherms at −196°C were obtained with a Micromeritics Gemini II 2370 apparatus. The sample was previously treated at 250 °C for 2 h under N_2 flow. The isotherms were elaborated by BET and α-plot methods, using the N_2 adsorption isotherm of non-porous silica as reference [29]. Micropore volumes and surface areas free from the contribution of micropores were calculated from the intercepts and the slopes of the α-plots. The accuracy of surface areas values was ±5%. Total pore volumes were determined from the amounts of adsorbed N_2 at $P/P^0 = 0.98$.

3. Results and discussion

3.1. Gel synthesis and structural characterisation

Gels were prepared hydrolysing TEOS in a solely aqueous acid environment according to a modified sol–gel method previously proposed [28]. It was shown that such method can lead to a better dispersion of an oxide in the

SiO_2 matrix [28]. In the present study, a lower TEOS:H_2O (1:4) molar ratio was used. This molar ratio corresponds to the stoichiometric one for the full hydrolysis of TEOS considering the reaction:

$$Si(OC_2H_5)_4 + 4H_2O = Si(OH)_4 + 4C_2H_5OH.$$

The product of this hydrolysis reaction undergoes subsequent polycondensation reactions producing siloxane bonds with ethanol and water as by-products. Therefore, the actual molar ratio required to obtain the siloxane network is less then 1:2 and the use of higher water amounts mainly affects the rate of the above reactions [28,30]. The addition of $Co(NO_3)_2 \cdot 6H_2O$ to the partially hydrolysed TEOS solution gives rise to a pinkish coloured solution that is indicative of the presence of the $[Co(H_2O)_6]^{2+}$ aquo-ion [31,32]. It is known that, in aqueous environment, this complex ion can undergo the acid–base equilibria forming Co oxo–hydroxo complexes that, in the presence of growing clusters containing hydroxo functionalities, $Si(OR)_x(OH)_y$, could give rise to condensation reactions forming Co–O–Si bridges [30,31]. According to our experimental approach the reaction medium is strongly acid, consequently the formation of Co complexes is strongly hindered and the probability of the formation of Co–O–Si bridges is very low. In these conditions, gelation is the result of polycondensation reactions involving the partially hydrolysed $Si(OR)_x(OH)_y$ oligomers. Therefore, all wet gels will be formed by a siloxane network in which the cobalt species are physically trapped. This hypothesis is confirmed by the pinkish colour of all wet gels as well as by the fact that all studied compositions exhibit the same gelation time (24 h) independently of the cobalt loading. This view is supported by the FT-IR results later on discussed.

Fig. 1 shows the TG/DTA curves of the dried gels with the derivative of the TG curves (DTG). The total weight losses given by the TG curves were: 24 wt% (10Co), 33 wt% (20Co) and 42 wt% (30Co). In each case, the majority of the weight loss takes place from room temperature to about 300 °C. In this range, for a typical gel-derived sample, the evaporation of the solvents and the subsequent pyrolysis and/or burning of residual organic molecules generally occur [30]. In the present case, the decomposition of the $Co(NO_3)_2 \cdot 6H_2O$ has to be taken into account as it happens between 27 and 327 °C ($T_d = 242$ °C) [33]. In this range, two poorly separated thermal effects are seen in the DTA curve of the 10Co sample. The endothermic peak with a maximum at 104 °C can be related to the evaporation, from open pores, of water and alcohol physically trapped in the gels. The exothermic peak with a maximum at 266 °C is likely to be caused by two overlapped processes: the burning of residual organic groups in the gels (exothermic) and the decomposition of the cobalt nitrate (endothermic). For 10Co the former process seems to be the faster one then covering the latter. The shift to lower temperature, 236 °C, of the corresponding DTG minimum gives a support to this observation.

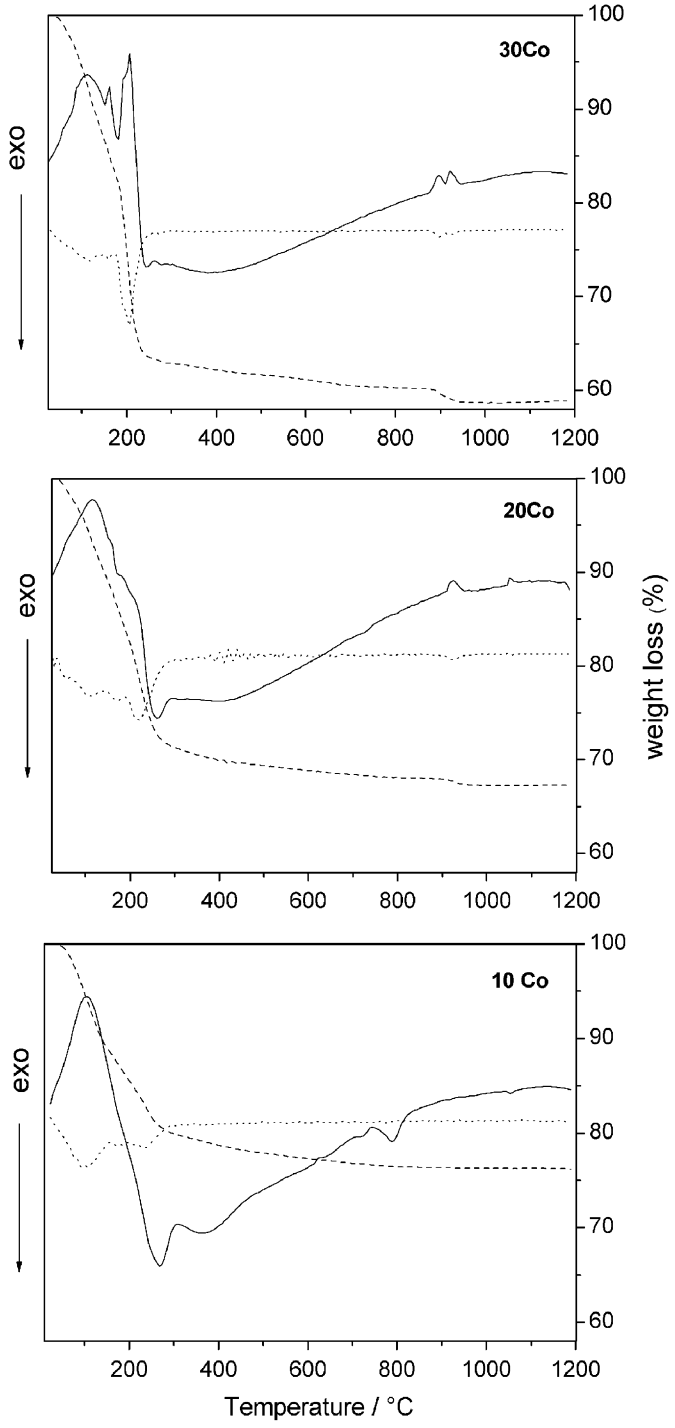

Fig. 1. DTA (solid line), TG (dashed line) and DTG (dotted line) curves of the dried gels recorded in air at 10 °C min^{-1}.

Interestingly, 30Co shows a different thermal behaviour. Its DTA curve shows two endothermic peaks: a broad peak from room temperature to about 180 °C, with a shoulder at 160 °C, followed by a sharp peak at 206 °C. At this temperature the corresponding DTG curve exhibits a sharp and very deep minimum related to a fast weight loss process: the decomposition of cobalt nitrate. 20Co resembles both the 10Co and 30Co samples. Actually, its

DTA curve shows a broad endothermic peak from room temperature to about 230 °C, with a maximum at 115 °C and two shoulders at about 160 and 200 °C, that is widely overlapped with an exothermic peak hardly visible at 260 °C. The corresponding DTG curve exhibits three minima at 115, 170 and 222 °C. Thus, for 20Co the above overlapped processes seem to occur to comparable rates.

An exothermic peak at 788 °C occurs in the DTA curve of 10Co and no weight loss is seen in the corresponding TG curve indicating that it can be related to a crystallisation phenomenon. In this temperature range no DTA exothermic peaks are detected in the curves of 20Co and 30Co. By contrast, these curves exhibit endothermic peaks at 923 °C (20Co), 897 °C and at 923 °C (30Co) and small weight losses, about 1% (20Co) and 2% (30Co) are seen in the corresponding TG curves. According to previous literature data [31,34], these peaks are related to the decomposition of the Co_3O_4, formed during the heating.

The structural evolution of dried gels upon heat treatments was studied by powder XRD as well as UV–vis and IR spectroscopy. The annealing temperatures, 400, 600 and 850 °C, were chosen on the basis of the thermal analysis data. The lower temperature stands for the minimum value at which it is possible to obtain complete decomposition of nitrate ions and elimination of the solvent and residual organics. The higher temperature values were selected to force the crystallisation of the samples.

The XRD patterns of the samples treated at 400 and at 850°C are reported in Fig. 2A and B, respectively. The 10Co—400 keeps its amorphous nature showing that the heat treatment does not lead to the formation of Co_3O_4, as expected from the decomposition of cobalt nitrate [35]. Consequently, in this sample the Co^{2+} ions are supposed to be strongly bonded to the siloxane matrix. On the contrary, the extent of the interaction between Co^{2+} ions and the siloxane matrix seems to be lower for the 20Co—400 and 30Co—400, allowing the crystallisation of the mixed valence cobalt oxide, Co_3O_4 (JCPDS card 42-1467) (Fig. 2A). It should be noted that for both samples the mean size of the Co_3O_4 crystallites resulted to be on the nanometric scale (about 13 nm), suggesting a high dispersion of the cobalt in the siloxane matrix.

At 850 °C the crystallisation of the Co_2SiO_4 phase (JCPDS card 15-0865) starts to occur, being the only crystallising phase for the 10Co—850 (Fig. 2B). For the 20Co—850 and 30Co—850, the presence of both Co_2SiO_4 and Co_3O_4 phases indicate that also in these samples there is a part of Co^{2+} ions that did not transform in Co_3O_4 during the stage at 400 °C because it is incorporated in the siloxane matrix. This strong interaction between Co^{2+} ions and the siloxane matrix explain the formation of the Co_2SiO_4 phase at 850 °C, likewise as occurs for the 10Co—400.

The room temperature diffuse reflectance UV–vis spectra of the dried gels and of the samples treated at 400 °C are shown in Fig. 3. The samples display different colours: violet for dried gels, blue for 10Co—400, black for the 20Co—400 and 30Co—400. The *d–d* transitions of Co^{2+} ions and the $O \rightarrow Co^{2+}$ charge transfer transitions are expected to occur in the visible and ultraviolet region, respectively [36]. In the visible region, the 10Co dried gel shows three bands at 525, 575 and 650 nm that are related to the $^4A_2$ (F)$\rightarrow ^4T_1$ (P) transition of $[Co(H_2O)_4]^{2+}$ complex [24,32,37]. The relative intensity of the triplet components does not correspond to the one of a typical complex ion in aqueous solution since the intensity of the component at 525 nm appears enhanced, while that of the component at 650 nm results to be reduced. Such type of distortion has been found in Co-containing mesoporous silica materials [38], zeolites [36] and silica gel [39] subject to dehydration–rehydratation processes. Either a partial coordination change from tetrahedral to octahedral, and hence the coexistence of both coordinations [36,38], or a change in ligand (OH groups and oxygen atoms of the siloxane matrix), and consequently distortion of tetrahedron [36], accounted for this observation. Increasing the Co loading, the presence in the dried gels of Co^{2+} ions in octahedral environment gets more and more visible. In 20Co spectrum broad band centred at about 530 nm with shoulders at about 490 and 650 nm are seen. In 30Co spectrum the absorbance at about 650 nm disappears where the presence of the broad absorbance peak at about 530 nm

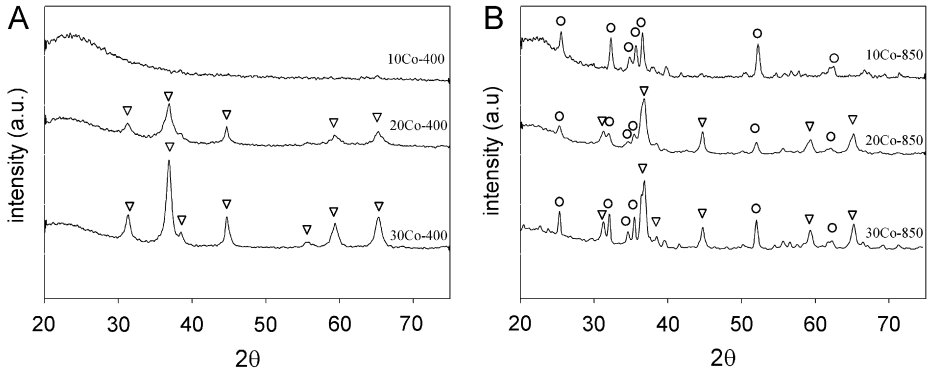

Fig. 2. XRD patterns of gel-derived samples at (A) 400 °C and (B) 850 °C. (○) Co_2SiO_4 (JCPDS card 15-0865). (▽) Co_3O_4 (JCPDS card 42-1467).

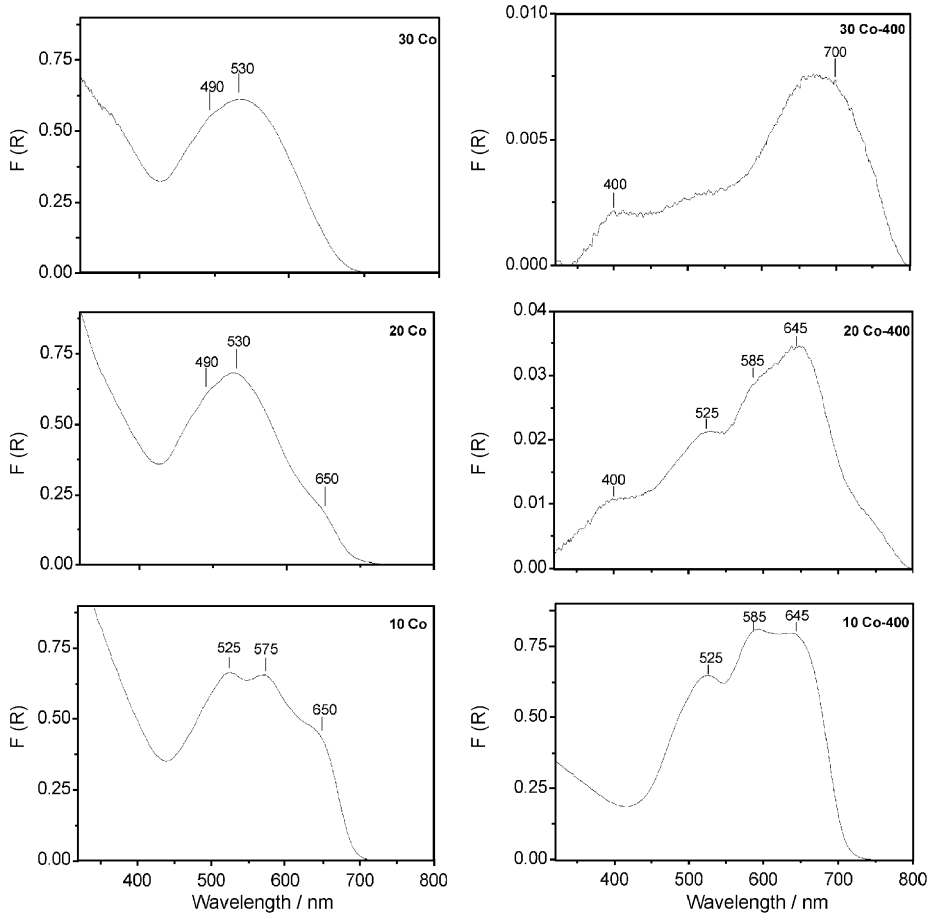

Fig. 3. UV–vis diffuse reflectance spectra of the dried gels and of the samples heat treated at 400 °C.

can be related to the highest energy transition $^4T_{1g}$ (F)→$^4T_{1g}$ (P) of Co^{2+} ions in octahedral environments [36]. As it is known, the intensity of this transition is lower than the one of the tetrahedral complex [36,40]. In spite of this, the spectra of all dried samples display comparable absorption values. This result, with the small difference of stability between tetrahedral and octahedral complexes of Co^{2+} ions [40], show that in all dried gels there is an equilibrium between the two kind of complexes that appear shifted towards the octahedral complex increasing the Co content.

The spectra of the samples heat treated at 400°C are strongly influenced by the extent of Co_3O_4 crystallisation degree. Thus, the spectrum of the amorphous 10Co—400 shows the typical triplet (525, 585 and 645 nm) commonly observed for the Co^{2+} ions in tetrahedral environment (Fig. 3). At this stage of heat treatment, the tetrahedral complex is likely to be $Co(OH)_4$ or CoO_4 where ligands come from silica matrix [32]. On the contrary, the spectra of the 20Co—400 and 30Co—400 mirror the partial oxidation of Co^{2+} to Co^{3+} with the simultaneous Co_3O_4 formation. In fact, in the UV–vis spectrum of the 30Co—400 the typical broad bands at about 400 and 700 nm related to the presence of the cobalt mixed valence oxide $[Co_2^{III}Co^{II}O_4]$ are seen [34,35,37]. The latter band displays in the low wavelength side some extent of absorption, suggesting the presence of not resolved features. On the other hand, features at about 525, 585 and 645 nm are clearly seen in the spectrum of the 20Co—400 with a broad band at about 400 nm (Fig. 3). These results point out the presence of two kinds of Co^{2+} ions in tetrahedral coordination: those belonging to Co_3O_4 phase and the framework-incorporated ones keeping the amorphous state.

FT-IR spectra of the dried gels are shown in Fig. 4. The narrow absorption band at 1385 cm^{-1} together with the weak band at 825 cm^{-1} confirm the presence of undecomposed nitrate ions in the network of all dried gels. In fact, the former band is related to the asymmetric stretching of N–O bonds in the NO_3^- units, the latter is related to the out-of-plane symmetric stretching of the same bonds [41]. Another common feature of the FT-IR spectra of dried gels is the envelope in the 1000–1300 cm^{-1} region. In this region the typical absorption bands of the siloxane network (1080, 1250 cm^{-1}) [42,43] are overlapped with some of the partially hydrolysed TEOS molecules (1168, 1082 cm^{-1}) [44]. Absorption bands at about 460 cm^{-1} (Si–O–Si bending vibrations) [44], 790 cm^{-1} (Si–O–Si symmetric

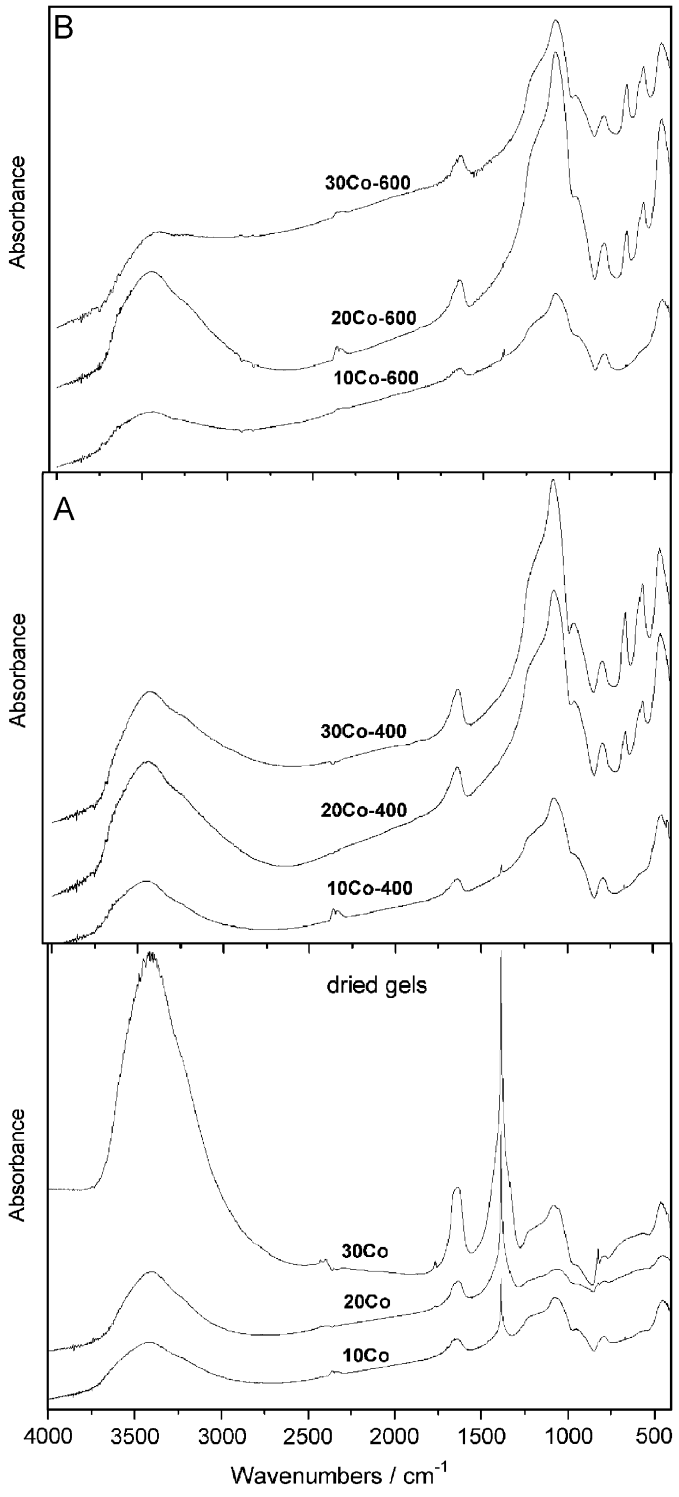

Fig. 4. FT-IR spectra of the cobalt containing samples: dried gels and of the samples treated at (A) 400 °C and (B) 600 °C.

stretching) [44] and 1650 cm^{-1} (deformation modes of O–H bonds and of molecularly adsorbed water) [45] are also seen with a broad absorption band in the 2750–3750 cm^{-1} range (stretching of O–H bonds) [44,45]. The maximum of this band occurs at about 3400 cm^{-1} for all dried gels, indicating the presence of hydroxyl groups involved in hydrogen-bonding of moderate strength [46], and the relative intensity changes with the Co content being the highest for the 30Co. A shoulder at about 950 cm^{-1}, more evident in the spectrum of 10Co sample, appears in FT-IR spectra of all dried gels. The assignment of this feature is a controversial point because it can be related to Si–OH and/or $Si–O^-$ stretching vibrations [37,44,46–48]. The formation of $Si–O^-$ groups appears to us probable in materials containing modifier and/or intermediate glass network oxides; on the other hand, in gel-derived materials containing only glass forming oxides this contribution must be considered not possible. In this case, the presence of cobalt oxide makes probable the formation of $Si–O^-$ groups and, consequently, the shoulder at about 950 cm^{-1} can be related to the stretching of $Si–O^-$ bonds. Taking into account the different intensities of the shoulders in the spectra of different samples, the interaction between Co^{2+} ions and the siloxane matrix seems to be stronger in the 10Co than in the other dried gels.

The structural evolution of dried gels on heating enhances the differences among the samples. In fact, the FT-IR spectra of the 20Co—400 and 30Co—400 display two absorption bands at 560 and 660 cm^{-1} that are related to the vibrations of Co(III)–O bonds in Co_3O_4, being those of Co(II)–O bonds IR active in the wavenumbers region lower than 400 cm^{-1} [49]. On the other hand, the spectrum of the 10Co—400 does not show these bands while still exhibits a low intensity band at 1385 cm^{-1}. Moreover, a shoulder at about 950 cm^{-1} is still evident in the spectrum of 10Co—400, whereas bands at 960 cm^{-1} appear in the spectra of the 20Co—400 and 30Co—400. This shift strengthens the above hypothesis that in the 10Co—400 there is a stronger interaction between Co^{2+} ions and the siloxane matrix with respect to 20Co—400 and 30Co—400 [48]. At the same time, a shoulder at about 3240 cm^{-1} visible in the FT-IR spectra of the samples heat treated at 400 °C attests the formation of OH groups involved in stronger hydrogen bonds [46]. Anyway, at this stage of heating, the highest absorption band occurs at 1080 cm^{-1} with a shoulder at about 1250 cm^{-1}, indicating that the dehydroxylation produces a more crosslinked siloxane framework.

The further heat treatment at 600 °C does not produce substantial structural changes except for the bands at about 950 and 3400 cm^{-1}. Actually, the former occurs at 965 cm^{-1} in the spectra of the 20Co—600 and 30Co—600 and its relative intensity appears slightly reduced with respect to the corresponding samples heated at 400 °C, while for the 10Co—600 it appears as more pronounced shoulder at lower wavenumbers (about 920 cm^{-1}). In the spectrum of the 30Co—600 the shape of the band at about 3400 cm^{-1} appears modified as consequence of the weaker absorption in the low wavenumbers side, while for the other gel-derived samples the shoulder at about 3420 cm^{-1} are more pronounced in some extent. These results can be considered as a consequence of the polycondensation of silanol groups occurring at this stage of the heat treatment [46].

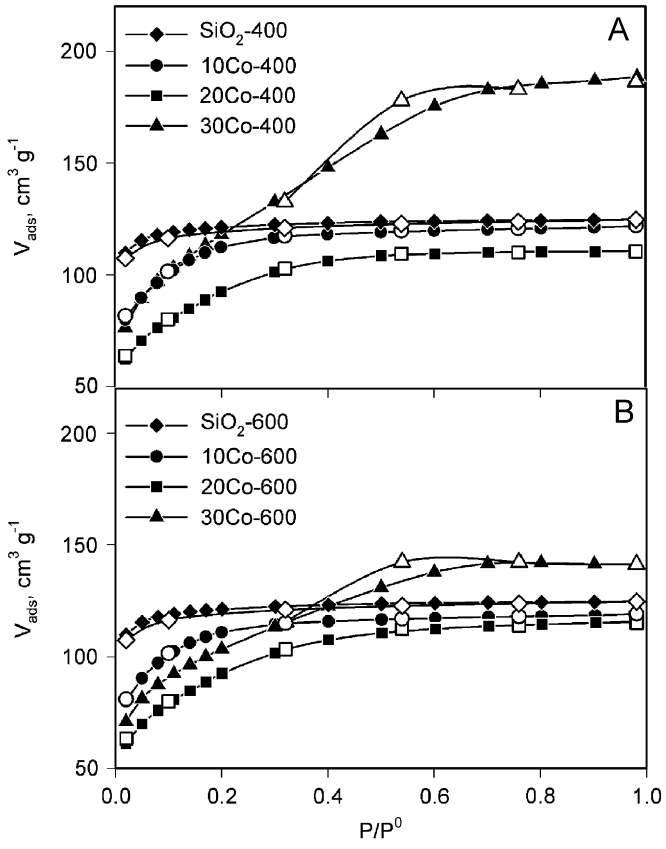

Fig. 5. N_2 adsorption–desorption isotherms of SiO_2 and samples treated at (A) 400 °C and (B) 600 °C. Full symbols: adsorption; empty symbols: desorption.

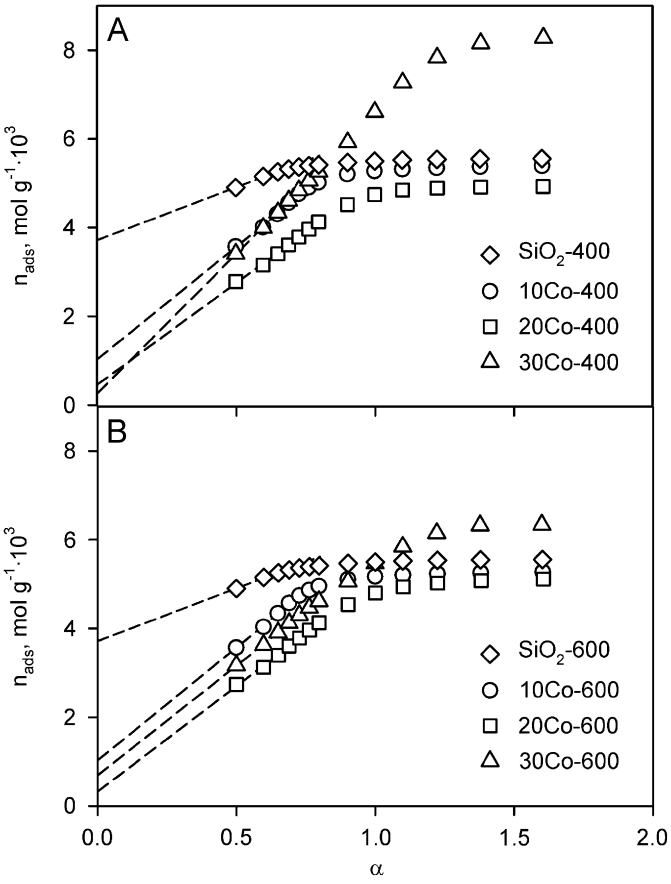

Fig. 6. α-Plots of SiO_2 and cobalt containing samples treated at (A) 400 °C and (B) 600 °C.

3.2. Textural properties

The N_2 adsorption–desorption isotherms of the samples heat treated at 400 and 600°C are reported in Fig. 5A and B, respectively, together with the ones of the correspondent silica samples. The isotherm of pure SiO_2—400, of type I according to the IUPAC classification [50], is characteristic of a microporous material, with high amounts of N_2 adsorbed at low pressures and a large plateau at $P/P^0 > 0.1$. The shape of the isotherms of 10Co—400 and 20Co—400 resembles that of SiO_2—400, however with plateau starting from higher P/P^0 values, suggesting the presence of microporosity also in these materials. On the other hand, the isotherm of 30Co—400, of type IV according to the IUPAC classification [50], is characteristic of a mesoporous material, with large adsorption volumes at $P/P^0 > 0.4$ and a desorption hysteresis. Increasing the temperature of the heat treatment to 600 °C the isotherms of SiO_2—600, 10Co—600 and 20Co—600 are not modified, while the isotherm of 30Co—600 is markedly modified, in the sense of decreasing N_2 adsorption (Fig. 5B). The adsorption isotherms are elaborated using, besides the conventional BET method, the α-plot one that is more advisable for materials containing micropores [29]. The corresponding α-plots reported in Fig. 6A and B appear typical of mesoporous–microporous materials [28] with an initial linear branch that gives a positive intercept proportional to the volume of micropores. Micropore volumes and surface areas calculated from α-plots are reported in Table 1 together with BET surface areas and total pore volumes. It can be observed that surface areas determined by α-plot are generally lower than those calculated by BET, especially for pure silica, because they exclude the contribution of micropores, with the exception of 30Co—400. For this sample BET and α-plot give same values indicating that microporosity is negligible. All the materials have BET

Table 1
Surface area, total pore volume and micropore volume of the studied samples

Sample	Surface area ($m^2 g^{-1}$)		Pore volume ($cm^3 g^{-1}$)	Micropore volume ($cm^3 g^{-1}$)
	BET	α-Plot		
SiO_2—400	401	151	0.193	0.129
10Co—400	409	322	0.198	0.036
20Co—400	314	291	0.171	0.016
30Co—400	411	413	0.288	0.009
SiO_2—600	405	150	0.190	0.128
10Co—600	404	323	0.185	0.036
20Co—600	316	302	0.179	0.016
30Co—600	368	314	0.219	0.024

surface areas close to that of pure silica, with the exception of samples 20Co—400 and 20Co—600 that show lower values. Total pore volumes of 10Co and 20Co heat-treated samples are close to that of pure SiO_2, but the presence of Co markedly affects the pore size distribution since the micropore volumes are lower than that of SiO_2 and regularly decrease with increasing Co content. Surface area and pore volume are almost independent from the temperature of thermal treatment, with exception of the samples with the highest Co content (Table 1). In fact, for these samples, the thermal treatment at 600 °C causes a large decrease of surface area and pore volume.

These data show that the presence of Co has the main effect of modifying the pore size distribution of silica, by reducing the micropore volume even at low Co content and adding some mesoporosity at the highest Co loading. These results can be related to the structural data reported above. Actually, it is clear that the incorporation of even low amounts of Co^{2+} reduces the microporosity of the silica framework because it affects the dehydroxylation mechanism.

The presence of the Co_3O_4 phase in 30Co—400 and 30Co—600, can explain their mesoporosity texture. It is known that a mesoporous Co_3O_4 is generally formed from decomposition of the Co nitrate at low temperature [51]. The dependence of surface area on Co content, with a minimum at 20Co, can be explained with two opposite effects. Increasing the Co content, the microporosity of silica decreases while the mesoporosity increases due to formation of the Co_3O_4 phase. The reduction of surface area and pore volume of 30Co—600 compared to those of 30Co—400 is probably due to partial sintering of Co_3O_4 phase at 600 °C.

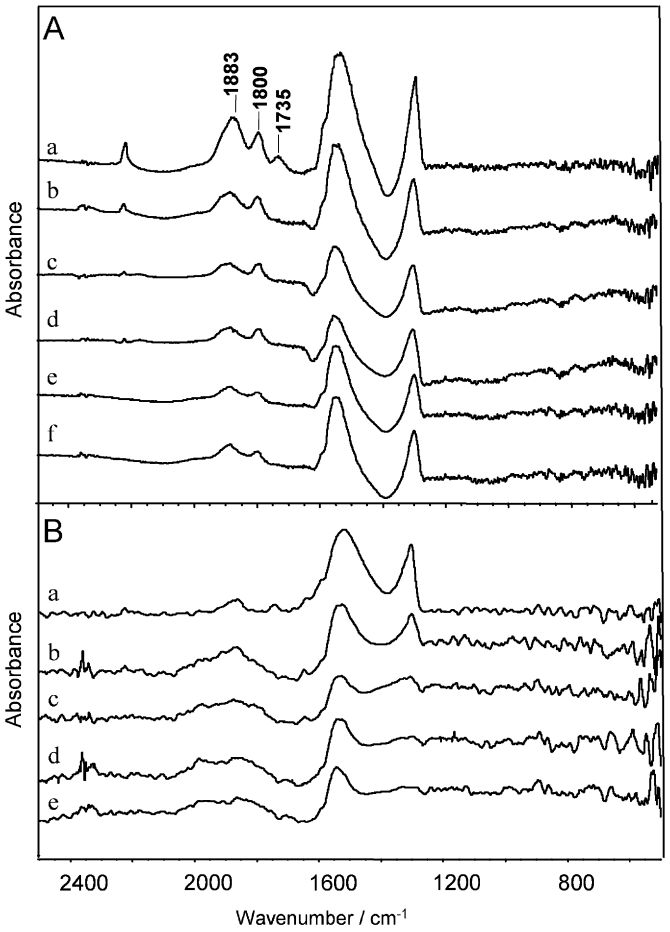

Fig. 7. (A) FT-IR subtraction spectra of 10Co after contact with NO gas at (a) room temperature, (b) 100 °C, (c) 200 °C, (d) 300 °C, after outgassing at (e) room temperature and (f) 200 °C. (B) FT-IR subtraction spectra of 30Co after contact with NO gas at (a) room temperature, (b) 100 °C, (c) 200 °C, after outgassing at (d) room temperature and (e) 100 °C.

3.3. Surface chemical properties

The nature of surface cobalt species has been investigated by FT-IR using NO as probe molecule. The adsorption of NO has been extensively investigated for the characterisation of cobalt oxide species [52]. In principle, NO can adsorb in a molecular form, giving rise to surface nitrosyls where it interacts with a lone pair of the N atom to the surface metal cationic centres, and can be oxidised by oxide surfaces, giving rise to species like nitrosonium ion (NO^+), nitrite ions (NO_2^-), adsorbed nitrogen dioxide (NO_2), nitronium ion (NO_2^+) and nitrate ions (NO_3^-). However, it can also act as an oxidising agent, reducing itself to NO^- and to its dimeric form, the hyponitrite anion ($N_2O_2^{2-}$), as well as to N_2O and N_2. Moreover, it can dimerise to dinitrogen dioxide N_2O_2 (which is possibly an intermediate in its reduction and/or in its oxidation) and disproportionate giving rise to both reduced and oxidised species. So nitrogen oxide is a probe molecule which provides detailed information about Lewis acidity and redox properties of cationic sites.

The adsorption of NO over 10Co at r.t., the following heating at increasing temperature and the outgassing at r.t. and 200 °C, give rise to the complex spectra reported in Fig. 7A. According to previous studies, the interaction of NO with supported cobalt-oxides [52–55] and supported cobalt–silica [56] is very complex and produces a number of different species, due to the reaction of NO, characterised by bands below 1800 cm^{-1}, and to molecularly adsorbed NO in the spectral range 1900–1800 cm^{-1}. A band at 1883 cm^{-1}, the intensity of which decreases after heating at 100 °C yet, due to NO weakly interacting with the surface and a weaker absorption at 1800 cm^{-1} are observed. These two bands suggest that NO coordinates over two different Lewis acid cationic sites, but an alternative assignment of the absorption at 1883 cm^{-1} to NO weakly interacting with the surface, probably through a hydrogen bond with the surface OHs, cannot be excluded. The position of the band at 1800 cm^{-1} is shifted to lower frequencies as compared to that of NO gas that shows a single band at 1875 cm^{-1}. The shift down of the NO stretching band of adsorbed nitrogen monoxide over metal oxides has been frequently observed and characterises terminal surface nitrosyl species, probably bent, where the π-type backbonding

from the *d*-orbitals of the adsorbing cation (partly filled) toward the π^* antibonding orbitals of NO predominates [52]. So the red shift of the NO stretching band of adsorbed nitrogen monoxide to 1800 cm^{-1} indicates the presence of terminal surface nitrosyl species adsorbed over Co^{2+} cations. However, the formation of Co^{2+} dinitrosyl cannot be excluded [57]. The absence of bands in the spectral region 1900–2200 cm^{-1} seems to exclude the presence of NO coordinated over Co^{3+} and of NO^+ species. A band, probably coupled, is also observed near 2224 cm^{-1}. This couple of bands, that disappears by outgassing at increasing temperature can be assigned to N-bonded and O-bonded species of adsorbed N_2O either formed on the surface from NO or present as an impurity in the gas [52,58].

In the spectral region below 1800 cm^{-1} the complex absorption in the 1600–1450 cm^{-1}, thermally more stable, is due mainly to different forms of bridged nitrates although presence of adsorbed NO_2 cannot be excluded. These species should be produced by NO oxidation. The assignment is not straightforward. On other oxides [59], these bands, that appear with another component near 1300 cm^{-1} have been assigned to the partially superimposed asymmetric and symmetric stretching modes of chelating NO_2^- nitrito ions. However, alternative assignments to species formed by NO reduction like hyponitrite species, as in *cis*-$K_2N_2O_2$, 1304 cm^{-1}, are more likely [52]. Since Co^{2+} species strongly interacting with the siloxane framework are hardly reducible [8,22], the formation of NO_2 or nitrate needs the contemporary formation of reduced species like hyponitrite ions according to the NO disproportionation reaction $3NO + O^{2-} = NO_2 + N_2O_2^{2-}$, also hypothesised for Mn/Al_2O_3 catalysts [59]. However, we cannot exclude the formation of a dinitrosyl species ON–Co–NO that could transform into $N_2O_2^{2-}$ hyponitrite ion. Finally, the band at 1735 cm^{-1} is likely due, probably together with the shoulder near 1450 cm^{-1}, to *cis*-N_2O_2.

The adsorption of NO at different temperature over 30Co gives rise to the complex spectra reported in Fig. 7B. The spectral behaviour is very similar to 10Co, but some significant differences can be detected. The first difference is a lower resolution of the spectra, due to the reduced transparency of the sample. This effect is clearly caused by light scattering, probably of Co_3O_4 particles present over the surface, as previously discussed. However, all the bands and their spectral feature at r.t. and after heating and outgassing observed over 10Co are still detectable. Moreover, a very weak and broad absorption near 2000 cm^{-1} can be detected. The bands that are usually attributable to linear Co^{n+}–NO species are two types: one above and one below 1900 cm^{-1}. Due to their weak intensity and the fact that they are typical of oxidised sample, it is common opinion that the bands above 1900 cm^{-1} are most probably due to NO adsorbed over Co^{3+} surface species [52]. So, FT-IR spectra of adsorbed NO over 30Co evidences the presence of Co^{3+} ions, but by effect of low resolution of the spectra we cannot understand if these ion are dispersed over the surface or in Co_3O_4 clusters. These observations, well agree with the presence of Co_3O_4 according to UV–vis and XRD data.

4. Conclusions

Cobalt–silicon mixed oxide nanocomposites characterised by a high dispersion of cobalt oxide species have been prepared by the modified sol–gel method tuned in this work. The nature of cobalt species and their interactions with the siloxane matrix are strongly depending on both the cobalt loading and the heat treatment. In the dried samples, an equilibrium between the tetrahedral and octahedral Co^{2+} complexes occurs that is shifted toward the octahedral form increasing the cobalt. At 400 °C, tetrahedral Co^{2+} complexes strongly bonded to the siloxane framework are found in the nanocomposite with the lowest cobalt content, while for the other ones besides these complexes Co_3O_4 nanocrystals are formed. At 850 °C, in all samples the crystallisation of the Co_2SiO_4 phase occurs, being the only crystallising phase for the nanocomposite with the lowest cobalt content. All materials show surface Lewis acidity, due to cationic sites, making them potential catalysts or gas sensors.

References

[1] N. Koshizaki, K. Yasumoto, T. Sasaki, Sens. Actuators B 66 (2000) 122–124.
[2] C. Cantalini, M. Post, D. Buso, M. Guglielmi, A. Martucci, Sens. Actuators B 108 (2005) 184–192.
[3] E. Ruckenstein, H.Y. Wang, Appl. Catal. A 204 (2000) 257–263.
[4] T.A. Kainulainen, M.K. Niemelä, A.O.I. Krause, Catal. Lett. 53 (1998) 97–101.
[5] S.W. Ho, J.M. Cruz, M. Houalla, D.M. Hercules, J. Catal. 135 (1992) 173–185.
[6] C. Ando, H. Kurokawa, H. Miura, Appl. Catal. A 185 (1999) L181–L183.
[7] E. Iglesia, Appl. Catal. A: Gen. 161 (1997) 59–78.
[8] B. Ernst, S. Libs, P. Chaumette, A. Kiennemann, Appl. Catal. A: Gen. 186 (1999) 145–168.
[9] K. Okabe, X. Li, T. Matsuzaki, H. Arakawa, K. Fujimoto, J. Sol–Gel Sci. Tech. 19 (2000) 519–523.
[10] C.L. Bianchi, F. Martini, P. Moggi, Catal. Lett. 76 (2001) 65–69.
[11] G. Jacobbs, T.K. Das, Y. Zhang, J. Li, G. Racoillet, B.H. Davis, Appl. Catal. A: Gen. 233 (2002) 263–281.
[12] J. Panpranot, S. Kaewkun, P. Praserthdam, J.G. Goodwin, J. Catal. Lett. 91 (2003) 95–102.
[13] A.Y. Khodalkov, R. Bechara, A. Griboval-Constant, Appl. Catal. A: Gen. 254 (2003) 273–288.
[14] P. Dutta, N.O. Elbashir, A. Manivannan, M.S. Seehra, C.B. Roberts, Catal. Lett. 98 (2004) 203–210.
[15] B.C. Dunn, D.J. Covington, P. Cole, R.J. Pugmire, Energy Fuels 18 (2004) 1519–1521.
[16] K. Okabe, X. Li, M. Wei, H. Arakawa, Catal. Today 89 (2004) 431–438.
[17] H.W. Lueke, Erdoel, Erdgas Kohle 121 (2005) 3–5.
[18] H. Boerrigter, A. van der Drift, DGMK Tagungsbericht 2 (2006) 49–56.
[19] B.C. Dunna, P. Cole, D. Covington, M.C. Webster, R.J. Pugmire, R.D. Ernst, E.M. Eyring, N. Shah, G.P. Huffman, Appl. Catal. A: Gen. 278 (2005) 233–238.

[20] I. Puskas, T.H. Fleisch, P.R. Full, J.A. Kaduk, C.L. Marshall, B.L. Meyers, Appl. Catal. A: Gen. 311 (2006) 146–154.
[21] Y. Zhang, K. Hanayama, N. Tsubaki, Catal. Commun. 7 (2006) 251–254.
[22] M.S. Ghattas, Microporous Mesoporous Mater. 97 (2006) 107–113.
[23] H. Li, S. Wang, F. Ling, J. Li, J. Mol. Catal. A: Chem. 244 (2006) 33–40.
[24] Y. Okamoto, K. Nagata, T. Adachi, T. Imanaka, K. Inamura, T. Takyu, J. Phys. Chem. 95 (1991) 310–319.
[25] Q. Tang, Q. Zhang, P. Wang, Y. Wang, H. Wan, Chem. Mater. 16 (2004) 1967–1976.
[26] C.L. Bianchi, V. Ragaini, Catal. Lett. 95 (2004) 61–65.
[27] T. Vraalstad, G. Oeye, J. Sjoeblom, M. Stoecker, J. Disp. Sci. Technol. 27 (2006) 489–496.
[28] A. Aronne, M. Turco, G. Bagnasco, P. Pernice, M. Di Serio, N.J. Clayden, E. Marenna, E. Fanelli, Chem. Mater. 17 (2005) 2081–2090.
[29] F. Rouquerol, J. Rouquerol, K. Sing, in: Adsorption by Powders and Porous Solids Principles, Methodology and Applications, Elsevier B.V., 1999.
[30] C.J. Brinker, S.W. Scherer, in: Sol–Gel Science: The Physics and Chemistry of Sol–Gel Processing, Academic Press, New York, 1990.
[31] G. Ortega-Zarzosa, C. Araujo-Andrade, M.E. Compeàn-Jasso, J.R. Martìnez, J. Sol–Gel Sci. Tech. 24 (2002) 23–29.
[32] K. Kojima, H. Taguchi, J. Matsuda, J. Phys. Chem. 95 (1991) 7595–7598.
[33] S. Yuvaraj, L. Fan-yuan, C. Tsong-Huei, Y. Chuin-Tih, J. Phys. Chem. B 107 (2003) 1044–1047.
[34] M. Zayat, D. Levy, Chem. Mater. 12 (2000) 2763–2769.
[35] G.A.H. Mekhemer, H.M.M. Abd-Allah, S.A.A. Mansour, Colloids Surf. A: Physochem. Eng. Aspects 160 (1999) 251–259.
[36] A.A. Verberckmoes, B.M. Weckhuysen, R.A. Schoonheydt, Microporous Mesoporous Mater. 22 (1998) 165–178.
[37] N. Martyanov, S. Uma, S. Rodrigues, K.J. Klabunde, Langmuir 21 (2005) 2273–2280.
[38] J. El Haskouri, S. Cabrera, C.J. Gomez-Garcia, C. Guillem, J. Latorre, A. Beltran, D. Beltran, M.D. Marcos, P. Amoros, Chem. Mater. 16 (2004) 2805–2813.
[39] A. Boos, G. Pourroy, J.L. Rehspringer, J.L. Guille, J. Non-Cryst. Solids 176 (1994) 172–178.
[40] F.A. Cotton, G. Wilkinson, C.A. Murillo, M. Bochmann, in: Advanced Inorganic Chemistry, sixth ed., Wiley, New York, 1999.
[41] C. Ehrhardt, M. Gjikaj, W. Brockner, Thermochim. Acta 432 (2005) 36–40.
[42] R.M. Almeida, T.A. Guiton, C.G. Pantano, J. Non-Cryst. Solids 121 (1990) 193–197.
[43] J. Gallardo, A. Durán, D. Di Martino, R.M. Almeida, J. Non-Cryst. Solids 298 (2002) 219–225.
[44] P. Innocenzi, J. Non-Cryst. Solids 316 (2003) 309–319.
[45] M. Cerruti, G. Magnacca, V. Bolis, C. Morterra, J. Mater. Chem. 13 (2003) 1279–1286.
[46] N.J. Clayden, S. Esposito, P. Pernice, A. Aronne, J. Mater. Chem. 12 (2002) 3746–3753.
[47] E. El-Malki, D. Werst, P.E. Doan, W.M.H. Sachtler, J. Phys. Chem. B 104 (2000) 5924–5931.
[48] M.S.P. Francisco, Y. Gushikem, J. Mater. Chem. 12 (2002) 2552–2558.
[49] K.J. Rao, H. Benqlilou-Moudden, B. Desbat, P. Vinatier, A. Levasseur, J. Solid State Chem. 165 (2002) 42–47.
[50] IUPAC Recommendations, Pure Appl. Chem. 57 (1985) 603–609.
[51] J. Van de Loosdrecht, A.M. Van der Kraan, M. Van der Haar, A.J. Van Dillen, J.W. Geus, Appl. Catal. A: Gen. 150 (1997) 365–376.
[52] K.I. Hadjiivanov, Catal. Rev. Sci. Eng. 42 (2000) 71–144.
[53] Y.J. Li, T.L. Slager, J.N. Armor, J. Catal. 150 (1994) 388–399.
[54] W.Z. Zhang, H. Yahiro, M. Iwamoto, J. Izumi, J. Chem. Soc. Faraday Trans. 91 (1995) 767–771.
[55] T. Montanari, O. Marie, M. Daturi, G. Busca, Catal. Today 110 (2005) 339–344.
[56] B. Djonev, B. Tsyntsarski, D. Klissursky, K. Hadjiivanov, J. Chem. Soc. Faraday Trans. 93 (1997) 4055–4063.
[57] K. Hadjiivanov, D. Klissursky, G. Ramis, G. Busca, Appl. Catal. B: Environ. 7 (1996) 251–267.
[58] M.A. Larrubia, G. Ramis, G. Busca, Appl. Catal. B: Environ. 30 (2001) 101–110.
[59] F. Kapteijn, L. Singoredjo, M. van Driel, A. Andreini, J.A. Moulijn, G. Ramis, G. Busca, J. Catal. 150 (1994) 105–116.